On the effects of dispersing polar nanoparticles in liquid crystals

INVITED ARTICLE

On the effects of dispersing polar nanoparticles in liquid crystals

Silvia Orlandi[a], Erika Benini[a], Matteo Ricci [a] and Claudio Zannoni[a]

[a]Dipartimento di Chimica Industriale "Toso Montanari", Università di Bologna, via Gobetti 85, 40129 Bologna, Italy

ARTICLE HISTORY
Compiled June 10, 2024

ABSTRACT
We have investigated the effect of adding polar rodlike nanoparticles (NPs) to a liquid crystal using Monte Carlo simulations. The mesogens (Ms) are represented with Gay-Berne elongated ellipsoids endowed with a central axial electric dipole. A NP is instead modelled by a overall rod-like set of rigidly assembled Lennard-Jones spherical beads [S. Orlandi et al., PCCP **18**, 2428 (2016)] that are either non-polar or endowed with a central axial dipole of different strengths. We consider two cases: one of strong NP-M affinity and weak NP-NP interactions (case 1) and the opposite one of weak NP-M affinity and strong NP-NP interactions (case 2). We find that for case 1 adding polar NPs slightly lowers the nematic-isotropic transition temperature T_{NI} which instead, for case 2, is essentially unaffected. Having strongly polar, instead of non-polar NPs reduces the T_{NI} difference with the pristine one, while significantly increasing the dielectric anisotropy in the nematic phase, which could be useful in applications.

KEYWORDS
Nanoparticles, liquid crystals, electric dipole effects, Monte Carlo simulations, Gay-Berne

1. Introduction

One of the fascinating aspects of liquid crystals (LCs) [1,2] is the variety of phases and physical properties they can exhibit by suitably changing the molecular structure of the constituent mesogens. Among the many ways of changing molecular organization in a controlled way, an important one is the introduction of an electric dipole moment at a chosen position and orientation of the mesogen molecular structure [3–6] by a suitable chemical substitution (or more than one of course). The technique is a powerful one, but presents unavoidable difficulties related to the mesogen synthesis and to the ability to control the changes in the macroscopic properties obtained, e.g. the dielectric constant or phase behaviour. An alternative, or just complementary, strategy for modifying LC properties, is based on adding and dispersing nanoparticles (NPs) to the mesophases [7–10]. This proves particularly effective since the resulting suspensions can exhibit

[*] dedicated to the memory of Professor Luis F. Rull, a pioneer of the computer simulations of liquid crystals, and to Professor José Luis Fernández Abascal on the occasion of his 70th birthday.

Contact: C. Zannoni. Email: claudio.zannoni@unibo.it; S. Orlandi. Email: s.orlandi@unibo.it

properties significantly different from those of the pure materials, while maintaining the optical transparency of key importance in optical applications, e.g. for LC displays (LCD), in view of the NPs size being much smaller than the visible light wavelength. A particularly interesting opening has been the possibility of forming regular self assembled suspensions of metallic (e.g. gold) nanoparticles to tailor the optical response, achieving metamaterials with very high or very low and negative values of refractive index, permittivity and/or permeability [11,12]. Adding semiconductor NPs, or quantum dots (QDs) is also of great technological importance [13]. In view of these and other applications, the field has been rapidly developing [10] but, while many experimental studies have appeared dealing with NP dispersions in LCs, as we can see from the numerous reviews [8,9,14–17] and recent papers [18,19], much less has been offered in terms of understanding the relation between NP properties and phase organizations, although with significant exceptions from theory [20–22] and computer simulations [23,24].

Two particularly interesting cases are that of NPs of different shape that we examined using computer simulations in [23] and that of polar NPs that we wish to treat here.

At the experimental level polar, paraelectric or ferroelectric nanoparticles have been added to LC [19,25–30]. The results are difficult to compare, as they refer to nanoparticles that can be of different size, shape, chemical nature and possibly with different stabilizing surfactant coating layers as well as different liquid crystals, pure or mixtures of different composition. Indeed, it is fair to say that the relation between a certain type of doping and the resulting changes in properties is far from clear. Modelling and computer simulations could be useful in this respect, by choosing a simple, but hopefully significative model system, both in terms of mesogen and nanoparticle shape and polarity and assessing the changes in phase transition and dielectric anisotropy, amongst the key target physical properties. Here we intend to proceed in this direction and explore the effects of the addition of polar NPs to a well studied model liquid crystal based on the Gay-Berne intermolecular potential [3] that presents nematic and smectic phases and examine the changes in phase behaviour and orientational order induced by the NPs as well as their dielectric.

2. Model

Many experiments performed on NP doped LC employ polar mesogens, like the very popular *n*-alkyl cyanobiphenyls or nCBs like 5CB and 8CB or commercial mixtures based on these systems (see, e.g. Table 1 in ref. [23]). Although pristine 5CB and 8CB have been simulated with atomistic details [31–35] a simulation of this type including NPs is not currently feasible and we have opted for a generic coarse grained approach as in [23]. More specifically e have modelled the mesogens as attractive-repulsive ellipsoids interacting with an heterogeneous generalization [3] of the Gay-Berne (GB) [2,36] potential, like in [23], but endowed here with a central axial dipole [37]. The nanoparticles are instead represented as elongated, rod-like, shaped rigid clusters of Lennard-Jones spheres (S) [23]. Each NP carries a dipole either located at the centre of the rod (see Fig. 1). Since the LJ spheres are just special cases of the GB ellipsoids, the heterogeneous GB allowing for different interacting ellipsoids can be used to handle the interaction

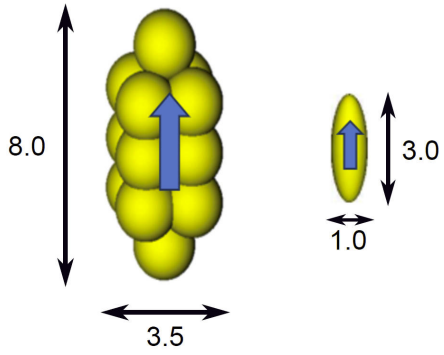

Figure 1.: Models of rod-like nanoparticle (left) formed by 14 LJ spherical beads and the ellipsoidal mesogen. The actual dimensionless length and breadth of the nanoparticle are also indicated. Assuming the mesogen to be similar to the typical polar mesogen showing a nematic and smectic phase 8CB, the effective dimensions of its ellipsoidal representation would be roughly $\sigma_0 \approx 0.6$nm (width) and 1.8nm (length) and then the nanoparticle length ≈ 4.8nm.

of the mesogens with each sphere belonging to the NPs.
The interaction between a pair of particles A, B is thus considered to be the sum of Gay-Berne (GB) and dipole-dipole (DD) interactions. The total interaction potential can be written as

$$\begin{aligned} U^{\mathrm{TOT}} &= \sum_{\mathrm{A}\neq\mathrm{B}} U_{\mathrm{AB}}^{\mathrm{TOT}} \equiv \sum_{\mathrm{A}\neq\mathrm{B}} U_{\mathrm{AB}}^{\mathrm{GB}} + U_{\mathrm{AB}}^{\mathrm{DD}} \\ &= \frac{1}{2}\sum_{\substack{i\in\mathrm{A}\\ j\in\mathrm{B}}} \left(U_{\mathrm{AB}}^{\mathrm{GB}}\right)_{ij} + \frac{1}{2}\sum_{\substack{i\in\mathrm{A}\\ j\in\mathrm{B}}} U_{ij}{}^{\mathrm{DD}}, \end{aligned} \tag{1}$$

where the particle pair types (AB) correspond to mesogen-mesogen (MM), nanoparticle-nanoparticle (NN), and heterogenous mesogen-nanoparticle (MN) or rather mesogen-bead (MS); . The generalized anisotropic Gay-Berne potential for two, possibly dissimilar particles i and j of type A, B (ellipsoids or LJ spheres) with orientations Ω_i, Ω_j (irrelevant for the spheres of course) separated by the centre-centre vector $\mathbf{r}_{ij}$ is [3].

$$\begin{aligned} \left(U_{\mathrm{AB}}^{\mathrm{GB}}\right)_{ij} &\equiv U_{\mathrm{AB}}^{\mathrm{GB}}(\Omega_i,\Omega_j,\mathbf{r}_{ij}) = 4\varepsilon_0\, e_{\mathrm{AB}}\epsilon_{\mathrm{AB}}^{(\mu\nu)}(\Omega_i,\Omega_j,\hat{\mathbf{r}}_{ij}) \\ &\times\left[\left(\frac{\sigma_c}{r_{ij}-\sigma_{\mathrm{AB}}(\Omega_i,\Omega_j,\hat{\mathbf{r}}_{ij})+\sigma_c}\right)^{12} - \left(\frac{\sigma_c}{r_{ij}-\sigma_{\mathrm{AB}}(\Omega_i,\Omega_j,\hat{\mathbf{r}}_{ij})+\sigma_c}\right)^{6}\right] \end{aligned} \tag{2}$$

where $\sigma_{\mathrm{AB}}(\Omega_i,\Omega_j,\hat{\mathbf{r}}_{ij})$ is a purely geometric pseudo-contact distance vector dependent on the shape anisotropy of A and B, with each ellipsoidal particle characterized by its three axes $\sigma_x^{(\mathrm{A})}$, $\sigma_y^{(\mathrm{A})}$ and $\sigma_z^{(\mathrm{A})}$, with σ_c an additional well width parameter, while the dimensionless interaction term $\epsilon_{\mathrm{AB}}^{(\mu\nu)}(\Omega_i,\Omega_j,\hat{\mathbf{r}}_{ij}) = \epsilon_{\mathrm{AB}}^{\nu}(\Omega_i,\Omega_j)\,\epsilon_{\mathrm{AB}}^{\prime\mu}(\Omega_i,\Omega_j,\hat{\mathbf{r}}_{ij})$, is related to the attractive energy anisotropy, with the model exponents μ and ν modifying the detailed form of the potential well [3]. The explicit expressions for the different contributions $\sigma_{\mathrm{AB}}(\Omega_i,\Omega_j,\hat{\mathbf{r}}_{ij})$, $\epsilon_{\mathrm{AB}}^{\nu}(\Omega_i,\Omega_j)$

and $\epsilon_{\mathrm{AB}}^{\prime\mu}\left(\Omega_i, \Omega_j, \hat{\mathbf{r}}_{ij}\right)$ are given in [2,3,38] and are not reported here for conciseness. For the homogeneous case, $\epsilon_{\mathrm{AA}}^{(\mu\nu)}$ is simply related to the potential well depths along the three molecular principal axis: $\varepsilon_x^{(\mathrm{A})}$, $\varepsilon_y^{(\mathrm{A})}$ and $\varepsilon_z^{(\mathrm{A})}$, while for the heterogeneous case a mixing rule introduced in [3] is adopted. The additional term e_{AB} is an affinity factor used to rescale the strength of the pair energy between particles of type A and B, while everything else remains the same [23]. We note that this is consistent with the rod-sphere form given in Ref. [9]. Properties are expressed in dimensionless units, labelled by asterisk, obtained by rescaling all quantities with respect to the characteristic length σ_0 and energy ε_0. In our specific case we arbitrarily assume $\sigma_0 = 0.6$ nm and $\varepsilon_0 = 1.0$kcal/mol.

The interactions between two dipoles i and j are calculated as

$$U_{ij}^{\mathrm{DD}} \equiv U_{ij}^{\mathrm{DD}}(\Omega_i, \Omega_j, \mathbf{r}_{ij}) = \frac{\mu_i \mu_j}{r_{\boldsymbol{\mu}_i \boldsymbol{\mu}_j}^3}\left[\hat{\boldsymbol{\mu}}_i \cdot \hat{\boldsymbol{\mu}}_j - 3(\hat{\boldsymbol{\mu}}_i \cdot \hat{\mathbf{r}}_{\boldsymbol{\mu}_i \boldsymbol{\mu}_j})(\hat{\boldsymbol{\mu}}_j \cdot \hat{\mathbf{r}}_{\boldsymbol{\mu}_i \boldsymbol{\mu}_j})\right] \tag{3}$$

where $\mathbf{r}_{\boldsymbol{\mu}_i \boldsymbol{\mu}_j}$ is the vector joining the point dipoles $\boldsymbol{\mu}_i$ and $\boldsymbol{\mu}_j$ on the particles A and B. In this paper we consider the dipole positioned at the centre of the mesogen or of the nanoparticles, thus $\mathbf{r}_{\boldsymbol{\mu}_i \boldsymbol{\mu}_j}$ corresponds also to distance vector $\mathbf{r}$. Here, and in the rest of the paper, we give the dimensionless dipole strength as $\mu^* \equiv \left(\mu^2/\epsilon_0 \sigma_0^3\right)^{1/2}$ where ϵ_0 and σ_0 are energy and length units prevously defined. The dipolar energy for particles in the box surrounded by its periodic images has been computed using the Reaction Field method, with cutoff $r_{RF}^* = 6.0$ for the system of pure mesogen or of the mesogen doped with non-polar NPs and cutoff $r_{RF}^* = 10.0$ for samples doped with polar NPs. In every case the dielectric constant of the surrounding medium was taken as $\epsilon_{RF} = 1.5$. Although this method is less rigorous than the Ewald summation one, it has previously proven in various works to be adequate for similar systems and sample sizes [4,39,40] while allowing significant advantages in terms of computation speed.

The parametrisation of the intermolecular potential and the thermodynamic conditions have been chosen in order to explore the range of temperatures in which the liquid crystals shows the transitions phases Isotropic-Nematic and Nematic-Smectic. We have assumed the mesogen to be uniaxial with $\sigma_x^{(\mathrm{M})} = \sigma_y^{(\mathrm{M})} = 1.0$ and $\sigma_z^{(\mathrm{M})} = 3.0$ (see Figure 1) and $\varepsilon_x^{(\mathrm{M})} = \varepsilon_y^{(\mathrm{M})} = 1.0$ and $\varepsilon_z^{(\mathrm{M})} = 0.2$. Each NP is modeled as a collection of 14 LJ spheres in which each sphere has $\sigma_{\mathrm{S}}^{(\mathrm{S})} = 2.0$ and different energetic terms $\varepsilon_{\mathrm{SS}}^{(\mathrm{S})} = 0.15$ and 2.0. For homogeneous interaction the affinity parameter e_{SS} and e_{MM} equal 1.0, while for the heterogeneous ones we have considered two different values $e_{\mathrm{MS}} = 0.5$ and 2.0 (see Figure 1). The GB model exponents have been set to $\mu = 2$ and $\nu = 1$[36,41].

As far as the nanoparticle-nanoparticle interactions are concerned, we see from the well depth that increasing $\varepsilon_{\mathrm{SS}}$ has the effect of making the *side-side* configuration significantly more attractive , which should favour the nanoparticles aggregation.

Lowering the affinity e_{MS} means that the interaction between nanoparticle and mesogen is disfavoured; as a consequence nanoparticle aggregation should also indirectly increase.

We have simulated mixtures of nanoparticles dispersed in a liquid crystal as detailed in the next section.

3. Systems Studied and Simulation Results

We have performed Monte Carlo simulations in the NPT ensemble with a constant dimensionless pressure $P^* = \sigma_0^3 P/\varepsilon_0 = 8.0$, performing cooling down sequences of runs starting from equilibrated isotropic configuration (we have explored a range of temperatures $1.0 < T^* < 1.8$ with $T^* = k_B T/\varepsilon_0$). We have investigated samples with a constant number of particles $N = N_{\rm N} + N_{\rm M} = 5000$ with 25 nanoparticles, corresponding to a 14% nanoparticle concentration in volume.

We have chosen an axial dimensionless dipole moment $\mu^*_{\rm M} = 1.5$ for the mesogen which, assuming, the parameters mentioned above corresponds to ≈ 5.5 Debye similar to that of cyanobiphenyls [32,33].

The parameter space for the system studied is very ample, consisting after the choice of the mesogen and of the nanoparticle shape, of the nanoparticle-nanoparticle interaction that we express in terms of interaction between the constituent spherical beads $\epsilon_{\rm SS}$, the mesogen-nanoparticle affinity $e_{\rm MS}$ and the nanoparticle dipole strength.

Here we specifically examined two cases for $e_{\rm SS}$ and $e_{\rm MS}$ and three nanoparticle dipoles: apolar ($\mu^*_{\rm N} = 0$) and polar ($\mu^*_{\rm N} = 5$) or very strongly polar ($\mu^*_{\rm N} = 20$) for the nanoparticle, corresponding to ≈ 18 or ≈ 73 Debye.

All initial configurations have been prepared by equilibrating at the same temperature and pressure, the $e_{\rm MS}$ was changed for every sample.

3.1. Case 1: Strong NP-mesogen affinity ($e_{\rm MS} = 2.0$) and weak NN interaction ($\epsilon_{\rm SS} = 0.15$).

In Figure 2 we show the pair potential profiles relative to the main interparticle approach directions (side-side, end-end and perpendicular) for mesogen-mesogen (MM) and nanoparticle-nanoparticle beads (SS), as well as for the heterogeneous interaction between nanoparticle and mesogen (NM). For dipolar particles we also report the curves for antiparallel (or parallel) dipolar orientations which provide an attractive (or repulsive) contribution to the total interaction energy.

The orientational order parameter is the most distinctive feature of LC and we are interested in seeing how it is affected by the addition of our NPs. We have thus computed the average values of the mesogen orientational order parameter

$$\langle P_2(\cos\beta)\rangle_{\rm M} = \left\langle \frac{3}{2}\cos^2\beta - \frac{1}{2} \right\rangle, \tag{4}$$

where the angular brackets indicate an average over equilibrium configurations, while β is the angle between mesogen long axis $\mathbf{u}$ and director $\mathbf{n}$, obtained setting up and diagonalizing an ordering matrix as described in detail in [2] . The simulation results are reported in Figure 3.

We see, for this system with bead-mesogen affinity $e_{\rm MS} = 2.0$, and bead-bead interaction strength $\varepsilon_{\rm SS} = 0.15$, that the addition of NPs does not change the phase sequence, but generally lowers in all cases the NI phase transition, with the major shift corresponding to non-polar and the smallest (inside error) deviation to the strongest dipole case.

An estimate of the clearing temperatures is $T^*_{NI} \approx 1.725 \pm 0.02$ for the pure mesogen, $T^*_{NI} \approx 1.625 \pm 0.02$ for the system with added non-polar nanoparticles, $T^*_{NI} \approx 1.675 \pm 0.02$ when the NP dipole is $\mu^*_{\rm N}$ =5 and $T^*_{NI} \approx 1.675 \pm 0.02$ for $\mu^*_{\rm N}$ =20.

Thus the clearing temperature is lowered in all cases by the addition of these type of nanoparticles of around 6% for apolar and 3% for both polar and strongly polar ones.

At low temperatures a nematic-smectic transition is observed. For the low temperature phase $\langle P_2 \rangle$ does not change much when changing dipole strength, and it is useful to plot , as in Figure 4 the pair density along the director, $g(z)$,

$$g(z) = \frac{1}{\pi R^2 \rho} \left\langle \delta \left(z - z_{12} \right) \right\rangle_{12} , \tag{5}$$

where $z_{12} = \boldsymbol{r}_{12} \cdot \hat{\boldsymbol{Z}}$ is measured with respect to the director frame, R is the radius of a cylindrical sampling region, ρ the density and the averages are computed over all the molecular pairs. We see from figure 4 that increasing the NP dipole from 5 to 20 increases the smectic character of the phase.

We have also calculated the mean square total dipole moment components parallel and perpendicular to the director: $\langle M_{\parallel}^{*} M_{\parallel}^{*} \rangle$ and $\langle M_{\perp}^{*} M_{\perp}^{*} \rangle$, where $\boldsymbol{M^*}$ is the instantaneous total electric dipole vector obtained summing over all polar particles (mesogens and nanoparticles) normalized to the number of particles

$$\boldsymbol{M}^{*} = \frac{1}{N} \sum_{i=1}^{N} \boldsymbol{\mu}_i^{*}, \tag{6}$$

These mean square components are related to the respective components of the low frequency dielectric constant tensor $\boldsymbol{\varepsilon}$ in the director frame. Converting the standard equation for the dielectric susceptivity [2] to dimensionless units ($k_B T / \epsilon_0 = T^{*}$), we have for the static dielectric tensor components of a non ferroelectric system ($\langle \boldsymbol{M^*} \rangle = 0$) containing only permanent dipoles [37,42,43]

$$\frac{3}{4\pi} (\varepsilon_{\parallel} - 1) V^{*} T^{*} = \langle M_{\parallel}^{*2} \rangle \tag{7a}$$

$$\frac{3}{4\pi} (\varepsilon_{\perp} - 1) V^{*} T^{*} = \langle M_{\perp}^{*2} \rangle . \tag{7b}$$

In Figure 5 we plot the results of the simulations for systems doped with NPs of different dipole strengths. Since these would correspond to different chemical systems, shifting the temperature of transition, we compare them plotting the results with respect to scaled temperature T^{*}/T_{NI}^{*}. We see a significant increase of the dielectric anisotropy resulting from the addition of the strongly polar NPs, with a relatively small change in the transition temperature.

It is interesting to compare the results with those predicted by Nordio, Rigatti and Segre [44] for the case of negligible intermolecular correlations ($\langle \mu_i \mu_j \rangle \approx 0$). In such situation, the dielectric constant components should reduce for molecular dipoles along the long axis to

$$\langle M_{\parallel}^{*2} \rangle = \langle \mu_{ZZ}^{*} \mu_{ZZ}^{*} \rangle = \mu_z^{*2} \left(\frac{1}{3} + \frac{2}{3} \langle P_2 \rangle \right) \tag{8a}$$

$$\langle M_{\perp}^{*2} \rangle = \frac{1}{2} \langle \mu_X^{*} \mu_X^{*} + \mu_Y^{*} \mu_Y^{*} \rangle = \mu_z^{*2} \left(\frac{1}{3} - \frac{1}{3} \langle P_2 \rangle \right) . \tag{8b}$$

where we use lower case or upper case subscripts for the vector components in the molecule or director frame respectively, In figure 6a we compare the two results. We that they are essentially superimposable indicating that the contribution of intermolecular cross terms is negligible.

We can also compare the total simulated dipole $\langle \boldsymbol{M^*}_{\mathrm{T}} \rangle$) for the suspension, with single particle counterpart calculated as

$$\langle (M^*_{\mathrm{T}})_{\parallel}{}^2 \rangle = x_M \mu_z^{*2} \left(\frac{1}{3} + \frac{2}{3} \langle P_2 \rangle_M \right) + x_N \mu_N^{*\,2} \left(\frac{1}{3} + \frac{2}{3} \langle P_2 \rangle_N \right) \tag{9a}$$

$$\langle (M^*_{\mathrm{T}})_{\perp}{}^2 \rangle = x_M \mu_z^{*2} \left(\frac{1}{3} - \frac{1}{3} \langle P_2 \rangle \right) + x_N \mu_N^{*\,2} \left(\frac{1}{3} - \frac{1}{3} \langle P_2 \rangle_N \right). \tag{9b}$$

where $x_M = N_M/N$ and $x_N = N_N/N$ are the mesogen and nanoparticle mole fractions. The results are shown in figure 6b.

3.2. Case 2: Weak NM affinity ($e_{\mathrm{MS}} = 0.5$) and strong NN interaction ($\epsilon_{\mathrm{SS}} = 2.0$).

Here we consider only the most interesting case of the strongest NP dipole, $\mu^*_{\mathrm{N}} = 20$. In Figure 7 we plot the pair potential for NN and NM interaction for this case. We see that the change in parameterization from case 1 to case 2 implies a much stronger NN attraction with the potential well down to nearly 60 units compared to around 12 for the side - side interactions.

We performed simulations to compare with the previous case for the same dipole strength. In Figure 8 we show the results for the order parameter as a function of temperature. From these it is apparent that the choice of weak nanoparticle-mesogen affinity and strong nanoparticle-nanoparticle interactions (case 2) brings the $\langle P_2 \rangle$ curve to practically coincide with the pristine LC one.

A calculation of the dielectric anisotropy yields the results in Figure 9, where we also compare them with the previous case of weak NN interaction and with the pure mesogen.

We see that the improvement on the dielectric anisotropy is similar for case 1 and case 2 for scaled temperatures higher than, say, 0.93, while at lower scaled temperatures the anistoropy for case 1 appears better.

4. Discussion and Conclusions

We have studied various composite systems formed by a polar mesogen doped with nanoparticles, formed by an assembly of Lennard-Jones spheres, having the same elongated shape but endowed with a central axial dipole of different strengths (0, 5, 20).

We have then considered two different kinds of nanoparticles that we imagine having, e.g. for their chemical nature and/or the type of stabilizing surface coating, either high nanoparticle-mesogen affinity and weak interaction between the nanoparticles (that we call case 1) or, viceversa, having weak nanoparticle-mesogen affinity and strong attractive interaction between nanoparticles (case 2). We have performed Monte Carlo simulations for systems of 25 NPs and 4975

Gay-Berne mesogens (volume concentration ≈ 14 %) that show:
i) The system that incorporates non-polar nanoparticles exhibits the greatest depression of the Nematic-Isotropic (N-I) transition temperature (which would correspond to some 20K for a real room temperature nematic) compared to systems containing dipolar nanoparticles.
ii) Systems with the strongest dipole closely approach the mesogen T_{NI} (within 3%) for case 1 and practically coincident for case 2.
iii) The dielectric anisotropy is significantly improved by the addition of strongly polar NPs.

It is not easy to compare our findings with real experiments, given the simplicity of our model, but it is interesting to try.

The effect on the T_{NI} of adding strongly polar NP has been experimentally studied for spherical $BaTiO_3$ in a nematic (5CB) and in a ferroelectric SmC by Dierking and collaborators [30]. Two nanoparticle types were considered: paraelectric (with size $\approx$ 50nm) and ferroelectric (size $\approx$ 240nm). They found that for the case of 5CB, the clearing point was not appreciably affected, while the dielectric anisotropy strongly increased for the ferroelectric NPs, in contrast to the constant values observed for the paraelectric ones. This indicates some similarity with our findings, even if the system is rather different from our one, also because of the different NP shape and concentrations. It is also interesting, even allowing for differences in nanoparticle size and concentration, that our findings are in accord with results of Herrington et al. [45] who found that the addition of $\mathrm{BaTiO_3}$ nanoparticles of size smaller than $50\ \mathrm{nm}$ to a nematic liquid crystal strongly increases the dielectric anisotropy. They showed that this leads in turn to a reduction of the voltage required for device driving and of the power consumption. This is important in the design of advanced liquid crystal devices utilizing nanoparticle dispersions in liquid crystals, as it points to how nanoparticle additives can be tailored to optimize these devices.

According to our simulations it appears that a way of obtaining such an optimized nematic dispersion of elongated strongly polar nanoparticles is to lower their interaction with the mesogenic host and increase the nanoparticle-nanoparticle interactions, as could probably be obtained varying and tuning the nanoparticle coating (often oleic acid derivatives) invariably used to stabilize the suspension. This optimization should allow an improved dielectric constant anisotropy while leaving the nematic-isotropic transition essentially unchanged with respect to the pristine mesogen.

Acknowledgements

We thank Victor Reshetnyak, Dean R. Evans and Isabella Miglioli for stimulating discussions on ferroelectric nanoparticles in a preliminary phase of this work.

Disclosure statement

No conflicts of interest to be declared.

References

[1] de Gennes PG, Prost J. The Physics of Liquid Crystals. Oxford: Clarendon Press; 1993.

[2] Zannoni C. Liquid Crystals and their Computer Simulations. Cambridge: Cambridge University Press; 2022.

[3] Berardi R, Fava C, Zannoni C. A Gay–Berne potential for dissimilar biaxial particles. Chem Phys Lett. 1998;297:8–14.

[4] Houssa M, Rull LF, McGrother SC. Effect of dipolar interactions on the phase behavior of the Gay-Berne liquid crystal model. J Chem Phys. 1998;109:9529–9542.

[5] Houssa M, McGrother SC, Rull LF. Computer simulations of dipolar liquid crystal phases. Comput Phys Comm. 1999;121:259–261.

[6] Berardi R, Orlandi S, Photinos DJ, Vanakaras AG, Zannoni C. Dipole strength effects on the polymorphism in smectic a mesophases. Phys Chem Chem Phys. 2002; 4:770–777.

[7] Shen Y, Dierking I. Perspectives in liquid crystal-aided nanotechnology and nanoscience. Applied Sciences-Basel. 2019;9.

[8] Singh S. Impact of dispersion of nanoscale particles on the properties of nematic liquid crystals. Crystals. 2019;9.

[9] Rastogi A, Mishra A, Pandey FP, Manohar R, Parmar AS. Enhancing physical characteristics of thermotropic nematic liquid crystals by dispersing in various nanoparticles and their potential applications. Emergent Materials. 2023;6:101–136.

[10] Lagerwall JP, Scalia G. Liquid Crystals with Nano and Microparticles. Vol. 7. World Scientific; 2016.

[11] Cai W, Shalaev V. Optical Metamaterials: Fundamentals and Applications. Springer; 2009.

[12] Draper M, Saez IM, Cowling SJ, Gai P, Heinrich B, Donnio B, Guillon D, Goodby JW. Self assembly and shape morphology of liquid crystalline gold metamaterials. Adv Funct Mater. 2011;21:1260.

[13] Qi H, Hegmann T. Formation of periodic stripe patterns in nematic liquid crystals doped with functionalized gold nanoparticles. J Mater Chem. 2006;16:4197.

[14] Choudhary A, George TF, Li GQ. Conjugation of nanomaterials and nematic liquid crystals for futuristic applications and biosensors. Biosensors-Basel. 2018;8.

[15] Kulkarni S, Kumar S, Thareja P. Colloidal and fumed particles in nematic liquid crystals: Self assembly, confinement and implications on rheology. J Mol Liq. 2021; 336.

[16] Kumar A, Priyam, Meena H, Prakash J, Wang L, Singh G. Recent advances on semiconducting nanomaterials-ferroelectric liquid crystals nanocomposites. J Phys Cond Matter. 2022;34.

[17] Ahmad F, Luqman M, Jamil M. Advances in the metal nanoparticles (MNPs) doped liquid crystals and polymer dispersed liquid crystal (PDLC) composites and their applications-a review. Mol Cryst Liq Cryst. 2021;731:1–33.

[18] Imamaliyev AR, Humbatov SA. Size effect of submicron barium titanate particles on dielectric properties of smectic A liquid crystal 4-nitrophenyl 4-decyloxy benzoate. Liq Cryst. 2023;50:1279–1286.

[19] Beigmohammadi M, Khadem Sadigh M, Poursamad J. Dielectric anisotropy changes in MBBA liquid crystal doped with barium titanate by a new method. Sci Rep. 2024; 14:5756.

[20] Lopatina LM, Selinger JR. Theory of ferroelectric nanoparticles in nematic liquid crystals. Phys Rev Lett. 2009;102:197802.

[21] Lopatina LM, Selinger JR. Maier-Saupe-type theory of ferroelectric nanoparticles in nematic liquid crystals. Phys Rev E. 2011;84:041703.

[22] Osipov MA, Gorkunov MV. Nematic liquid crystals doped with nanoparticles: Phase behavior and dielectric properties. In: Lagerwall JPF, Scalia G, editors. Liquid crys-

tals with nano and microparticles. Vol. 1; Chapter 3; Singapore: World Scientific; 2017. p. 135–175.
[23] Orlandi S, Benini E, Miglioli I, Evans DR, Reshetnyak V, Zannoni C. Doping liquid crystals with nanoparticles. a computer simulation of the effects of nanoparticle shape. Phys Chem Chem Phys. 2016;18:2428–41.
[24] Angioletti-Uberti S. Theory, simulations and the design of functionalized nanoparticles for biomedical applications: A soft matter perspective. NPJ Computational Materials. 2017;3.
[25] Buchnev O, Dyadyusha A, Kaczmarek M, Reshetnyak V, Reznikov Y. Enhanced two-beam coupling in colloids of ferroelectric nanoparticles in liquid crystals. J Opt Soc Am B. 2007;24:1512.
[26] Lin Y, Daoudi A, Dubois F, Blach JF, Henninot JF, Kurochkin O, Grabar A, Segovia-Mera A, Legrand C, Douali R. A comparative study of nematic liquid crystals doped with harvested and non-harvested ferroelectric nanoparticles: phase transitions and dielectric properties. RSC Advances. 2017;7:35438–35444.
[27] Garbovskiy Y, Glushchenko A. Ferroelectric nanoparticles in liquid crystals: Recent progress and current challenges. Nanomaterials. 2017;7.
[28] Basun SA, Cook G, Reshetnyak VY, Glushchenko AV, Evans DR. Dipole moment and spontaneous polarization of ferroelectric nanoparticles in a nonpolar fluid suspension. Phys Rev B. 2011;84.
[29] Cook G, Barnes JL, Basun SA, Evans DR, Ziolo RF, Ponce A, Reshetnyak VY, Glushchenko A, Banerjee PP. Harvesting single ferroelectric domain stressed nanoparticles for optical and ferroic applications. J Appl Phys. 2010;108:064309.
[30] Al-Zangana S, Turner M, Dierking I. A comparison between size dependent paraelectric and ferroelectric batio3 nanoparticle doped nematic and ferroelectric liquid crystals. J Appl Phys. 2017;121.
[31] Cacelli I, De Gaetani L, Prampolini G, Tani A. Liquid crystal properties of the n-alkyl-cyanobiphenyl series from atomistic simulations with ab initio derived force fields. J Phys Chem B. 2007;111:2130–2137.
[32] Tiberio G, Muccioli L, Berardi R, Zannoni C. Towards in silico liquid crystals. realistic transition temperatures and physical properties for n-cyanobiphenyls via molecular dynamics simulations. ChemPhysChem. 2009;10:125–136.
[33] Palermo MF, Pizzirusso A, Muccioli L, Zannoni C. An atomistic description of the nematic and smectic phases of $4n$-octyl-4' cyanobiphenyl (8CB). J Chem Phys. 2013; 138:204901.
[34] De Gaetani L, Prampolini G. Computational study through atomistic potentials of a partial bilayer liquid crystal: structure and dynamics. Soft Matter. 2009;5:3517–3526.
[35] Zhang J, Su J, Guo H. An atomistic simulation for 4-cyano-4 '-pentylbiphenyl and its homologue with a reoptimized force field. J Phys Chem B. 2011;115:2214–2227.
[36] Gay J, Berne B. Modification of the overlap potential to mimic a linear site-site potential. J Chem Phys. 1981;74:3316.
[37] Berardi R, Orlandi S, Zannoni C. Antiphase structures in polar smectics liquid crystals and their molecular origin. Chem Phys Lett. 261;363–368:1996.
[38] Ricci M, Roscioni OM, Querciagrossa L, Zannoni C. MOLC. a reversible coarse grained approach using anisotropic beads for the modelling of organic functional materials. Phys Chem Chem Phys. 2019;21:26195–26211.
[39] Gil-Vilegas A, McGrother S, Jackson G. Reaction-field and Ewald summation methods in Monte Carlo simulations of dipolar liquid crystals. Mol Phys. 1997;92:723.
[40] Berardi R, Orlandi S, Zannoni C. Monte Carlo simulations of rod-like Gay-Berne mesogens with transverse dipoles. Int J Mod Phys C. 1999;10:477–484.
[41] De Miguel E, Rull LF, Chalam MK, Gubbins KE. Liquid crystal phase diagram of the Gay-Berne fluid. Mol Phys. 1991;74:405.
[42] Kusalik PG. Computer simulation results for the dielectric properties of a highly

polar fluid. J Chem Phys. 1990;93:3520–3535.
[43] Sanchez H. Uncertainties in the static dielectric constants computed from molecular dynamics simulations. J Mol Liq. 2019;288:111021.
[44] Nordio PL, Rigatti G, Segre U. Dielectric relaxation theory in nematic liquids. Mol Phys. 1973;25:129–136.
[45] Herrington MR, Buchnev O, Kaczmarek M, Nandhakumar I. The effect of the size of $BaTiO_3$ nanoparticles on the electro-optic properties of nematic liquid crystals. Mol Cryst Liq Cryst. 2010;527:72.

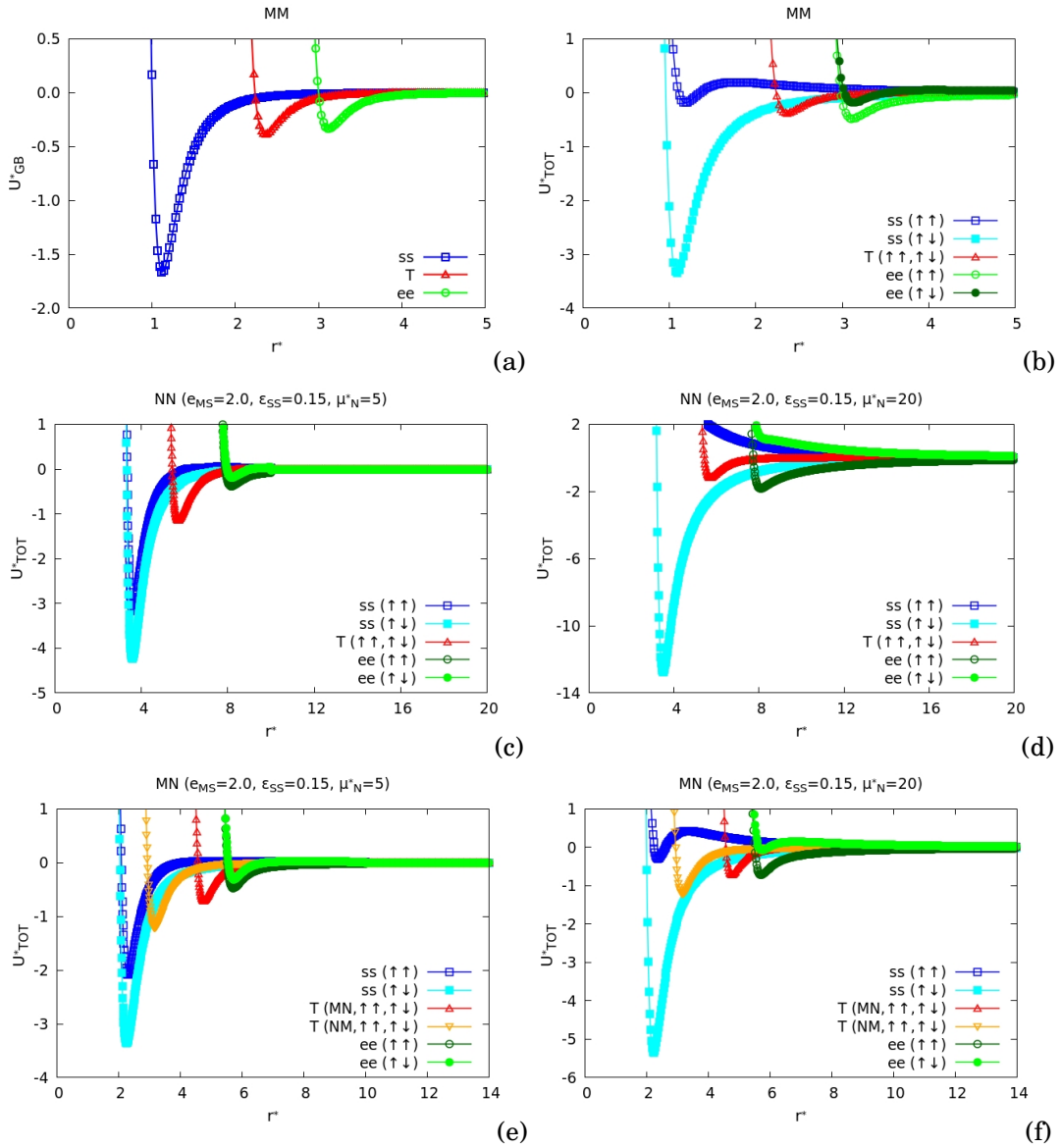

Figure 2.: On the top line, Gay-Berne (a) and total, Gay-Berne plus dipolar (b) pair potential energy curves for mesogen-mesogen (MM) interactions. Middle line shows the total pair potential for nanoparticle-nanoparticle (NN) with the nanoparticle dipole $\mu^*_{\rm N} = 5$ (c) and 20 (*d*). The bottom line shows the analogous curves for mesogen-nanoparticles (MN) (e), (f). We represent side-side (ss), T-like (T), end-end (ee) configurations for parallel and antiparallel dipole orientations. The curves are shown for the choice of bead-mesogen affinity $e_{\rm MS} = 2.0$, and bead-bead interaction strength $\varepsilon_{\rm SS} = 0.15$ employed for the simulations.

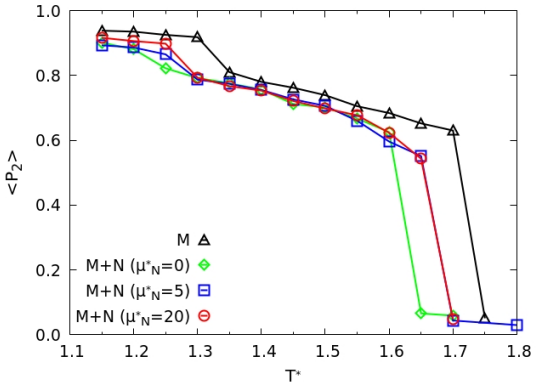

Figure 3.: Temperature dependence of the orientational order parameter $\langle P_2 \rangle$ of the mesogen particles for the pure liquid crystal (triangle) and for the system with added nanoparticles with a dipole $\mu^*_{\mathrm{N}} = 0$ (diamond), $\mu^*_{\mathrm{N}} = 5$ (squares), $\mu^*_{\mathrm{N}} = 20$ (circles). Here the bead-mesogen affinity is "strong": $e_{\mathrm{MS}} = 2.0$, and the bead-bead interaction "weak": $\varepsilon_{\mathrm{SS}} = 0.15$.

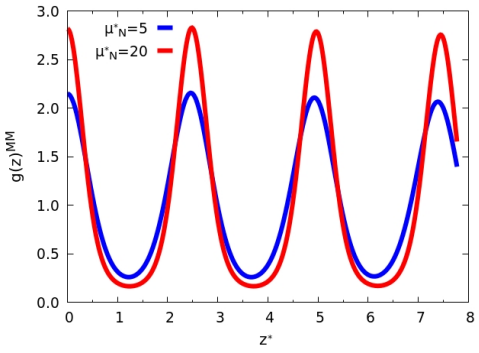

Figure 4.: Pair correlation function along the director $g(z^*)$ at a temperature ($T^* = 1.15$) in the smectic phase showing the onset of better defined layers as the NP dipole increase from $\mu^*_{\mathrm{N}} = 5$ to 20.

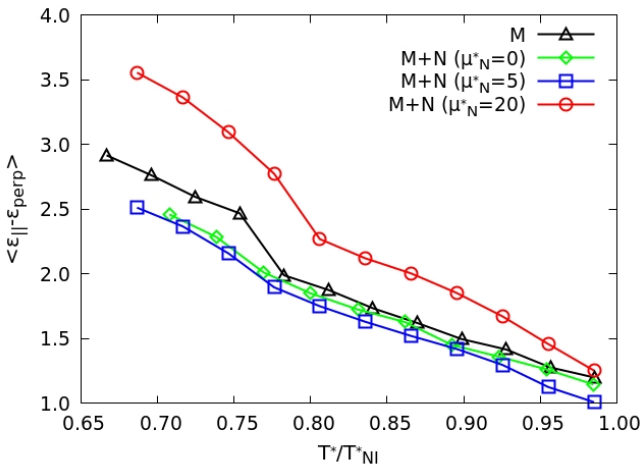

Figure 5.: Dielectric constant tensor components for the system of pure mesogens and for samples doped with polar nanoparticles of different dipole strength for case 1, as indicated in the inset. To facilitate comparison we plot the results vs scaled temperatures T^*/T^*_{NI}.

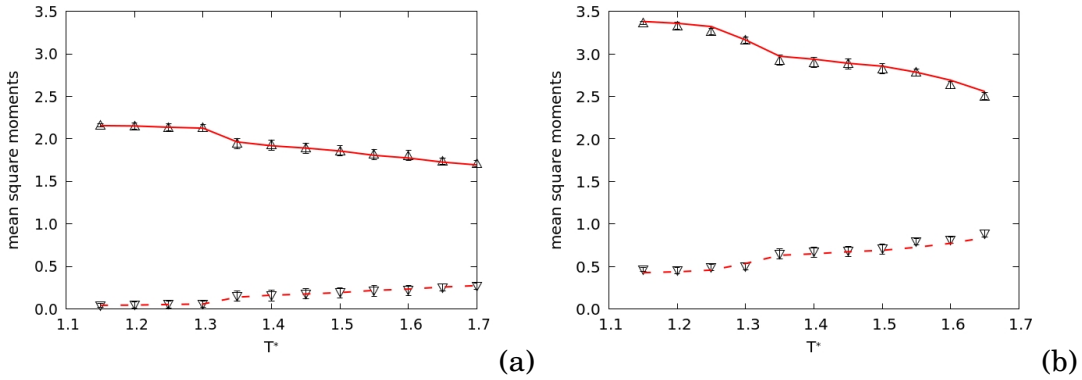

(a) (b)

Figure 6.: Left: Comparison between simulated overall mean square total dipole moment of the mesogens parallel, $\langle M^{*2}_{\parallel}\rangle$, ($\triangle$) and perpendicular, $\langle M^{*\,2}_{\perp}\rangle$ ($\triangledown$) to the director and the single molecule mean square ones calculated from Nordio-Rigatti-Segre theory [44] in Eqs. 8 (respectively continuous and dashed red lines). Right: the same for the mean square total dipole moment of the NP suspension (see Eqs. 9).

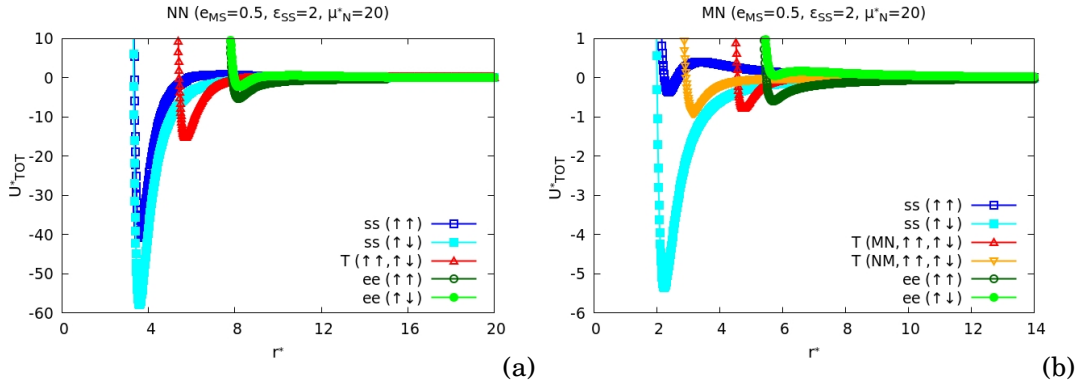

Figure 7.: Total Gay-Berne plus dipolar pair potential energy curves for bead-mesogen affinity $e_{\mathrm{MS}} = 0.5$, and bead-bead interaction strength $\varepsilon_{\mathrm{SS}} = 2.0$ and the bead dipole $\mu^*_{\mathrm{N}} = 20$ for NN (a) and NM (b). We represent side-side (ss), T-like (T), end-end (ee) configurations for parallel and antiparallel dipole orientations.

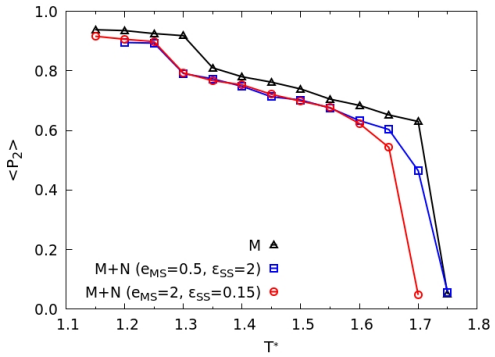

Figure 8.: Temperature dependence of the orientational order parameter $\langle P_2 \rangle$ for the mesogen particles for the pure liquid crystal (triangle) and for the system with added nanoparticles with a dipole $\mu^*_{\mathrm{N}} = 20$ for different affinity (case 1 and 2).

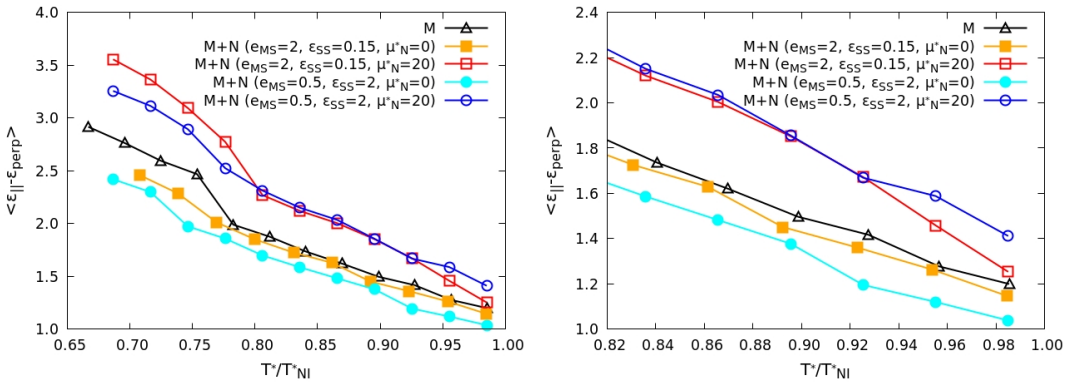

Figure 9.: Dielectric anisotropy for samples doped with polar nanoparticles of the same dipole strength ($\mu^*_{\mathrm{N}} = 20$) and NN and NM interactions corresponding to case 1 and case 2 as indicated in the inset. The curves for both systems doped with non-polar nanoparticles and for the sample of pure mesogen are shown for comparison. On the left the full temperature range, on the right a close up on the nematic region.